Prateek Gupta[1]
Supreet Singh Bahga[2]

[1]ETH Zürich, Department of Mechanical and Process Engineering, Zürich, 8092, Switzerland
[2]Department of Mechanical Engineering, Indian Institute of Technology Delhi, New Delhi, India

Received September 9, 2020
Revised November 22, 2020
Accepted December 3, 2020

Research Article

High-resolution numerical simulations of electrophoresis using the Fourier pseudo-spectral method

We present the formulation, implementation, and performance evaluation of the Fourier pseudo-spectral method for performing fast and accurate simulations of electrophoresis. We demonstrate the applicability of this method for simulating a wide variety of electrophoretic processes such as capillary zone electrophoresis, transient-isotachophoresis, field amplified sample stacking, and oscillating electrolytes. Through these simulations, we show that the Fourier pseudo-spectral method yields accurate and stable solutions on coarser computational grids compared with other nondissipative spatial discretization schemes. Moreover, due to the use of coarser grids, the Fourier pseudo-spectral method requires lower computational time to achieve the same degree of accuracy. We have demonstrated the application of the Fourier pseudo-spectral method for simulating realistic electrophoresis problems with current densities as high as 5000 A/m^2 with over tenfold speed-up compared to the commonly used second-order central difference scheme, to achieve a given degree of accuracy. The Fourier pseudo-spectral method is also suitable for simulating electrophoretic processes involving a large number of concentration gradients, which render the adaptive grid-refinement techniques ineffective. We have integrated the numerical scheme in a new electrophoresis simulator named SPYCE, which we offer to the community as open-source code.

Keywords:
High-resolution / Nonlinear electrophoresis / Pseudo-spectral method / Simulations
DOI 10.1002/elps.202000259

Additional supporting information may be found online in the Supporting Information section at the end of the article.

1 Introduction

Numerical simulation has become an indispensable tool for understanding the fundamental behaviour and optimisation of various electrophoresis techniques such as CZE [1], isotachophoresis (ITP) [2], field-amplified sample stacking (FASS) [3,4], and IEF [5]. Early work on simulations of electrophoresis, beginning with the work of Bier et al. [6], focused on understanding the dynamics of electrophoretic techniques and the role of various physical and chemical processes in separation and preconcentration of ionic species. With ever-increasing computational power and availability of free simulations tools, such as SIMUL [7] and SPRESSO [8], electrophoresis techniques can now be simulated on personal computers by anyone having a basic understanding of electrophoresis. Therefore, numerical simulations have now found applications in: (i) exploring optimal process parameters for improved separation and preconcentration of analytes, (ii) development of new electrophoretic assays, (iii) and teaching [9]. Recent advances in the understanding of electrophoresis phenomena, for example, the discovery of oscillating electrolytes [10,11] and development of advanced electrophoresis assays, such as those based on bidirectional ITP [12–14], have been made possible primarily by numerical simulations.

Numerical simulations of electrophoresis are based on solving the coupled transport equations for ionic species

Correspondence: Dr. Supreet Singh Bahga, Department of Mechanical Engineering, Indian Institute of Technology Delhi, New Delhi, India.
E-mail: bahga@mech.iitd.ac.in

Abbreviations: **1D**, one-dimensional; **DFT**, discrete Fourier transform; **FASS**, field-amplified sample stacking; **FFT**, fast Fourier transform; **LE**, leading electrolyte; **ODEs**, ordinary differential equations; **RKF45**, fourth-order Runge–Kutta–Fehlberg method; **SLIP**, symmetric limited positive scheme; **SPYCE**, pseudo-spectral Python code for electrophoresis; **TE**, trailing electrolyte; **tITP**, transient-ITP

Color online: See article online to view Figs. 1–4 in color.

including the effects of electromigration, advection due to bulk flow, diffusion, and chemical equilibria. Beginning with the early work of Bier et al. [6] and Saville and Palusinski [15] on the modelling of electrophoretic techniques, various improvements to the mathematical model of electrophoresis have been made. These include, modelling of protein mobility [16], ionic-strength dependence on electrophoretic mobility [17], Taylor-Aris dispersion [8,18], and axially varying channel cross-section [18]. Most of the modern numerical simulators for electrophoresis, such as SIMUL [7], SPRESSO [8, 18], and GENTRANS [19], are based on the one-dimensional (1D) or quasi-1D formulation of the governing equations proposed by Saville and Palusinski [15] with some or all of the aforementioned improvements in the mathematical model. A review and comparison of the capabilities of these simulators have been presented by Thormann et al. [9,20]. In contrast to the abovementioned simulators, which can simulate nonlinear electrophoresis systems, electrophoresis techniques, such as zone electrophoresis and electrokinetic chromatography, can also be simulated using the linearised species transport equations. This simulation approach, based on the linear theory of electromigration, has been implemented in the PeakMaster simulator [21]. Besides dedicated 1D simulators for electrophoresis, multiphysics simulation packages, such as OpenFOAM [22] and COMSOL [23, 24], enable both 1D and multidimensional simulations of a variety of nonlinear electrophoresis techniques.

While the available simulators and published studies on electrophoresis simulations are based on similar mathematical models, they differ primarily in the choice of the numerical method, particularly the spatial discretization scheme. The spatial discretization schemes for numerically solving the transport equations for electrophoresis can be broadly classified into dissipative and nondissipative schemes. The dissipative schemes, such as upwind scheme [25], flux-corrected transport scheme [26], and symmetric limited positive scheme (SLIP) [18] incorporate artificial numerical diffusion to ensure stability and prevent spurious oscillations in the solution. The dissipative schemes yield stable, nonoscillatory solutions even on coarser computational grids but at the expense of lower accuracy. Such schemes are perfectly suited for performing rough, exploratory simulations for the design of electrophoretic assays. The flux corrected transport scheme and the SLIP scheme have been integrated in GENTRANS [26] and SPRESSO [18] simulators, respectively. On the other hand, the nondissipative schemes, such as the second-order central difference [27] and sixth-order compact schemes [8], offer significantly higher accuracy due to the absence of numerical diffusion. However, these spatial discretization schemes require a relatively finer grid to ensure stable nonoscillatory solutions. The most commonly used nondissipative scheme is the second-order central difference scheme which has been implemented in SIMUL and GENTRANS simulators. The SPRESSO simulator allows a choice between second-order central difference and sixth-order compact schemes, besides the dissipative SLIP scheme.

One way to address the drawbacks of low accuracy of the dissipative schemes and the requirement of high grid density of the nondissipative schemes is to use adaptive grid refinement. For example, Bercovici et al. [8] demonstrated the use of adaptive grid refinement to perform high-resolution simulations of electrophoresis using the sixth-order compact scheme, with lesser number of grid points and correspondingly lower computational time. On the other hand, Bahga et al. [18] used the adaptive grid refinement for improving the accuracy of the unconditionally stable SLIP scheme, particularly in the regions with large concentration gradients. These adaptive grid-refinement schemes have been integrated in the open-source SPRESSO simulator. The adaptive grid refinement techniques, however, require a careful choice of grid-refinement parameters to be effective in stabilising the nondissipative schemes or improve the accuracy of dissipative schemes. An improper choice of grid-refinement parameters can lead to excessive computational time in dynamically adapting the grid, thereby negating the benefit of adaptive grid refinement. This is particularly true if a small number of grid points are used while simulating electrophoretic processes with sharp gradients or for systems, such as oscillating electrolytes, where a large number of concentration gradients are distributed throughout the computational domain.

An alternate approach of achieving high accuracy with relatively low grid density is to use pseudo-spectral methods [28,29]. Unlike, the finite difference and the finite-volume methods that are based on spatially local approximations of a function with low-order polynomials, the pseudo-spectral methods are based on global representations of a function such as the Fourier series or high-order polynomials [28–30]. Pseudo-spectral methods offer accuracy unmatched by other local methods and permit use of a coarser grid. Pseudo-spectral methods are exceptionally successful for simulating naturally periodic problems involving convective and wave phenomena. Moreover, physical problems that are not naturally periodic, such as initial-value problems, can also be solved on a periodic domain. For these reasons, pseudo-spectral methods have found applications in various disciplines including meteorology [31], geophysics [32], fluid dynamics [33], and acoustics [34]. All electrophoresis techniques involve wave-type phenomena and can be formulated as initial value problems [35–37]. Therefore, pseudo-spectral methods are perfectly suited for simulating electrophoresis techniques on coarser computational grids with high accuracy. Despite these advantages, till date application of pseudo-spectral methods for simulating electrophoretic processes has not been demonstrated.

In the current work, we demonstrate the application of a particular type of pseudo-spectral method called the Fourier pseudo-spectral method for performing fast and accurate simulations of a variety of electrophoretic processes including CZE, oscillating electrolytes, FASS, and transient-ITP (tITP) [14]. In particular, we show that the Fourier pseudo-spectral method yields accurate numerical

solutions of electrophoresis problems for realistic current densities, with a lesser number of grid points and lower computational time. We benchmark our simulations with the experimentally validated SPRESSO solver that uses the sixth-order compact scheme. To highlight the advantages of the Fourier pseudo-spectral method, we compare the results from the pseudo-spectral method with those using the nondissipative, second-order central difference scheme. The numerical scheme presented in this article allows for electrophoresis simulations only on a periodic domain. We show that a variety of electrophoresis techniques, except ITP, moving boundary electrophoresis and IEF, can be simulated in a periodic framework. We note that nonperiodic problems can also be simulated using other types of pseudo-spectral methods, and we will report the application of such methods to electrophoresis in the near future. For the benefit of electrophoresis community, we offer our pseudo-spectral method-based electrophoresis simulator as an open-source code, written in Python programming language. The simulator is named SPYCE (Pseudo-spectral Python Code for Electrophoresis) and is available for free download at http://web.iitd.ac.in/~bahga/SPYCE.html.

2 Material and methods

2.1 Mathematical model

We consider a 1D mathematical model for transport of ionic species in a capillary or microchannel due to advection, electromigration, and diffusion. The governing equations describing electrophoretic transport of weak electrolytes have been discussed in detail by Hruška et al. [7] and Bercovici et al. [8], and are briefly reviewed here. The cross-sectional area-averaged, total (analytical) concentration of species family i, denoted by c_i, varies along the axial coordinate x and time t as

$$\frac{\partial c_i}{\partial t} + \frac{\partial}{\partial x}\left(uc_i + \mu_i E c_i\right) = \frac{\partial^2}{\partial x^2}\left(D_i c_i\right), \quad i = 1, \ldots, m. \tag{1}$$

Here u denotes the axially-uniform mean velocity of the bulk fluid, μ_i the effective mobility, D_i the effective diffusivity, and E the local electric field. The total concentration of species family i is the sum of concentrations $c_{i,z}$ of various ionisation states (denoted by the valence state$z$),

$$c_i = \sum_{z_i=n_i}^{p_i} c_{i,z}. \tag{2}$$

Here n_i and p_i denote the minimum and maximum valence states for species family$i$. For example, for arginine, the valance states are $z = -1, 0, 1, 2$and hence $n_i = -1$ and $p_i = 2$. In Eq.(1), the effective mobility μ_i and effective diffusivity D_i are defined as the weighted mean of mobilities and diffusivities of various ionisation states z of $i-$th species with ionisation fractions $g_{i,z}$ as the weights,

$$\mu_i = \sum_{z=n_i}^{p_i} \mu_{i,z} g_{i,z}, \quad D_i = \sum_{z=n_i}^{p_i} D_{i,z} g_{i,z}, \quad g_{i,z} = \frac{c_{i,z}}{c_i}. \tag{3}$$

In the current work, we ignore the effects of ionic strength of electrophoretic mobility, which can be incorporated in a straightforward manner, as shown by Bahga et al. [17].

In typical electrophoresis experiments, the species transport occurs at timescales that are significantly longer compared with those of acid-base dissociation reactions [15]. Therefore, knowing the total concentrations c_i of all the species, the concentrations of various ionisation states $c_{i,z}$ can be obtained by assuming local chemical equilibrium. The chemical equilibrium calculations have been described in detail by Hruška et al. [7] and Bercovici et al. [8]. Here, we follow the same approach to obtain concentrations $c_{i,z}$ and concentrations of hydronium ionc_H and hydroxyl ionc_{OH}, knowing the total concentrations c_i of all the species families. The chemical equilibrium calculations rely on the relation between concentrations of two consecutive ionisation states with the equilibrium constants $K_{i,z}$, as $c_{i,z}c_H/c_{i,z+1} = K_{i,z}$and the electroneutrality condition given by

$$c_H - c_{OH} + \sum_{i=1}^{m}\sum_{z=n_i}^{p_i} z c_{i,z} = 0. \tag{4}$$

In addition, the concentrations of hydronium and hydroxyl ions are related by $c_H c_{OH} = K_w$, where K_w is the ionic product of water.

The species transport equations (Eq. (1)) for various species $i = 1, \ldots, m$ are coupled through the local electric field E,which is governed by the conservation of current. For a constant current density χ, the local electric field is given by

$$E = \frac{1}{\sigma}\left(\chi + \frac{\partial S}{\partial x}\right), \tag{5}$$

where σ denotes the local electrical conductivity and $\partial S/\partial x$ denotes the diffusive current density. These quantities are given by

$$\sigma = F\left(\mu_H c_H - \mu_{OH} c_{OH} + \sum_{i=1}^{m}\sum_{z=n_i}^{p_i} z\mu_{i,z} c_{i,z}\right) \tag{6}$$

and

$$S = F\left(D_H c_H - D_{OH} c_{OH} + \sum_{i=1}^{m}\sum_{z=n_i}^{p_i} z D_{i,z} c_{i,z}\right), \tag{7}$$

where F is the Faraday's constant. In Eqs. (6) and (7), the subscripts H and OH denote the physical quantities of hydronium and hydroxyl ions, respectively. Substituting the expression for local electric field E given by Eq. (5) in Eq. (1), we arrive at the coupled set of m partial differential equations

which we solve numerically,

$$\frac{\partial c_i}{\partial t} + \frac{\partial}{\partial x}\left(uc_i + \frac{\mu_i \chi}{\sigma} c_i\right) + \frac{\partial}{\partial x}\left(\frac{\mu_i c_i}{\sigma}\frac{\partial S}{\partial x}\right) = \frac{\partial^2}{\partial x^2}\left(D_i c_i\right), \quad i = 1, \ldots, m. \tag{8}$$

2.2 Fourier pseudo-spectral method

In the Fourier pseudo-spectral method, hereafter referred to as the FPS method, we numerically solve the set of governing equations, Eq. (8), in Fourier (or wavenumber) space rather than in physical space [28,29]. The transformation from the physical space to the Fourier space is given by the Fourier Transform. The Fourier transform of any spatially varying physical quantity $f(x, t)$, defined on a real line, such as concentration and conductivity, is defined as

$$\hat{f}(k, t) \triangleq \mathcal{F}\left\{f(x, t)\right\} = \int_{-\infty}^{\infty} f(x, t) e^{-jkx} \mathrm{d}x, \tag{9}$$

where k is the wavenumber and $j = \sqrt{-1}$. The conversion from the Fourier space to physical space is given by the inverse Fourier transform,

$$f(x, t) \triangleq \mathcal{F}^{-1}\left\{\hat{f}(k, t)\right\} = \frac{1}{2\pi}\int_{-\infty}^{\infty} \hat{f}(k, t) e^{jkx} \mathrm{d}k, \tag{10}$$

Next, we apply the Fourier transform to both sides of the governing equations, Eq. (8), to get

$$\frac{\mathrm{d}\hat{c}_i}{\mathrm{d}t} + jk\mathcal{F}\left(uc_i + \frac{\mu_i \chi}{\sigma} c_i\right) + jk\mathcal{F}\left(\frac{\mu_i c_i}{\sigma}\mathcal{F}^{-1}\left(jk\mathcal{F}(S)\right)\right) = -k^2\mathcal{F}\left(D_i c_i\right), \quad i = 1, \ldots, m. \tag{11}$$

Here, we have used the differentiation property of the Fourier transform, that is,$\mathcal{F}(df/dx) = jk\mathcal{F}(f)$and $\mathcal{F}(d^2 f/dx^2) = -k^2\mathcal{F}(f)$, to express the transform of derivative terms. Note that, the diffusion current term in Eq. (11) results from the fact that $\partial S/\partial x = \mathcal{F}^{-1}(jk\mathcal{F}(S))$. The differentiation property of Fourier transform converts the coupled set of partial differential equations in the physical space, Eq. (8), to a set of nonlinear ordinary differential equations (ODEs), Eq. (11), in the Fourier space. The resulting ODEs in time, Eq. (11), are solved numerically to obtain the Fourier coefficients $\hat{c}_i(k, t)$. Thereafter, the inverse Fourier transform given by Eq. (10) is used to obtain the concentrations in the physical space.

In practice, for computer implementation of the above-mentioned procedure one works with a finite periodic domain and use the Discrete Fourier Transform (DFT) instead of the continuous Fourier transform. The DFT is computed using the computationally-efficient Fast Fourier Transform (FFT) algorithm. For further details on the implementation of the FPS method, the readers are referred to excellent texts by Trefethen [28] and Boyd [29] and the open-source code of SPYCE. Here, we briefly outline the numerical procedure. We begin by discretizing the computational domain into$N$ grid points, $x_k = k\Delta x$ where $k = 0, 1, \ldots, N-1$, $\Delta x = L/N$, and L is the length of the domain in physical units. We assume the problem to be periodic, that is, the value of any spatially varying physical quantity at x_0 is equal to that at $x_N = N\Delta x = L$. The initial conditions in physical space are transformed to the Fourier space using the DFT, and the resulting ODEs, similar to Eq. (11)) are solved numerically to estimate the coefficients of DFT at the next time-step. In the current work, we use the fourth-order Runge–Kutta–Fehlberg (RKF45) adaptive time-stepping scheme for numerically solving the resulting ODEs. After each time-step, the concentrations in the physical space are computed using the inverse DFT, and these concentrations are used to perform chemical equilibrium calculations to determine the local $\mathrm{pH} = -\log_{10}(c_H[M])$, effective mobilities and diffusivities using Eq.(3), and conductivity using Eq. (6). Thereafter, the same procedure is repeated for subsequent time-steps. We note that the computation of nonlinear terms in Eq. (11) leads to aliasing errors and associated loss in accuracy [29]. To avoid aliasing errors, we use the Fourier smoothing method of Hou and Li [38] wherein we multiply the DFT coefficients of concentrations at the end of every time-step with a weighting function to attenuate high wavenumbers. Hou and Li [38] showed the effectiveness of such low-pass filtering on capturing nonlinear diffusive wave propagation (Burgers equation), which is also the nature of wave propagation phenomena in electrophoresis [36].

The FPS method described above works for only periodic problems. Although the requirement of periodicity appears to be limiting, as we shall show later in Section 3, a variety of electrophoresis techniques can be simulated on a periodic grid. This is because the conditions at the left and the right boundaries in many electrophoresis techniques are identical and do not vary with time. Exceptions to this are electrophoresis techniques, such as ITP, moving boundary electrophoresis, and IEF, where the ends of the channel are filled with different electrolytes. Such nonperiodic problems can be solved numerically using other types of pseudo-spectral methods, such as the Chebyshev pseudo-spectral method. We will report the application of such methods for performing numerical simulations of nonperiodic problems in a future article.

We implemented the numerical algorithm discussed above in Python 3.0 programming language using the NumPy library. To demonstrate the accuracy and computation time of simulations based on FPS method, we also implemented the second-order central difference scheme, hereafter referred as CD2 scheme, in a similar Python code. The chemical equilibrium calculations were verified separately with the SPRESSO simulator. All simulations were performed on Intel i7 1.8 GHz, 16 GB RAM personal computer with Ubuntu 18.04 operating system.

3 Results and discussion

In this section, we present simulations of various electrophoretic processes, such as CZE, t-ITP, and oscillating electrolytes, using the FPS method and their comparison with the simulations using the CD2 scheme. In addition, we present verification of our numerical implementation

of the FPS method in the SPYCE simulator with the sixth-order compact scheme implemented in SPRESSO. Besides these simulations, in the Supporting Information, we show the applicability of our numerical method for simulating FASS. We note that a detailed comparison of various spatial discretization schemes for simulating electrophoresis, including the upwind, CD2, sixth-order compact, and SLIP schemes, has been provided elsewhere [8,18]. Moreover, the advantages of the FPS method over other finite difference schemes have been well documented in the literature [28,29]. Our focus in this section is to demonstrate the ability of the FPS method to simulate a wide variety of electrophoretic processes. To highlight the accuracy and speed-up offered by the pseudo-spectral method, throughout we compare its performance with the CD2 scheme, which is the most popular numerical scheme for electrophoresis.

3.1 Capillary zone electrophoresis (CZE)

We begin by presenting simulations of a benchmark problem of CZE, proposed originally by Ermakov et al. [39] and subsequently adopted in various numerical studies of electrophoresis [8,18,26]. Simulations were performed for a 200 mm long, 50 μm diameter circular capillary filled with a BGE consisting of 12 mM tris ($pK_a = 8.076$ and $\mu = 29.5 \times 10^{-9}$ m^2/Vs) and 20 mM acetic acid ($pK_a = 4.756$ and $\mu = -42.4 \times 10^{-9}$ m^2/Vs). The analytes, aniline ($pK_a = 4.8$ and $\mu = 32.5 \times 10^{-9}$ m^2/Vs) and pyridine ($pK_a = 5.16$ and $\mu = 30 \times 10^{-9}$ m^2/Vs), were initially present in the form of Gaussian-shaped zones with a variance of 12.5 mm^2, centered at a distance of 30 mm from the left end of the capillary. We performed two sets of simulations corresponding to both analytes having initial concentrations of 10 μM and 1 mM. All simulations were performed at a constant current of 5 μA (current density of 2547 A/m^2). The first case with 10 μM initial concentration of analytes involves linear electromigration of analyte peaks and allows comparison of the numerical solution with the analytical solution. Whereas, the second case with 1 mM initial concentration of analytes involves strong electromigration dispersion of analyte peaks and was chosen to test the ability of the FPS method to resolve sharp concentration gradients. For both these cases, we compared the results of simulations using the FPS method, CD2 scheme, and the sixth-order compact scheme with an adaptive grid (1000 grid points) implemented in SPRESSO. In addition to these simulations, in the Supporting Information, we present simulations of electrophoretic separation of the same analytes with sample stacking using FASS.

Figures 1A and B show the simulated concentrations of fullyseparated analytes at $t = 200$ s, for the cases with initial analyte concentrations of 10 μM and 1 mM, respectively. To simulate the linear case with 10 μM initial analyte concentrations, 1024 grid points were used, whereas for the nonlinear case with 1 mM initial analyte concentrations 4096 grid points were used to resolve the sharp concentration gradients. At low analyte concentrations, shown in Fig. 1A, the

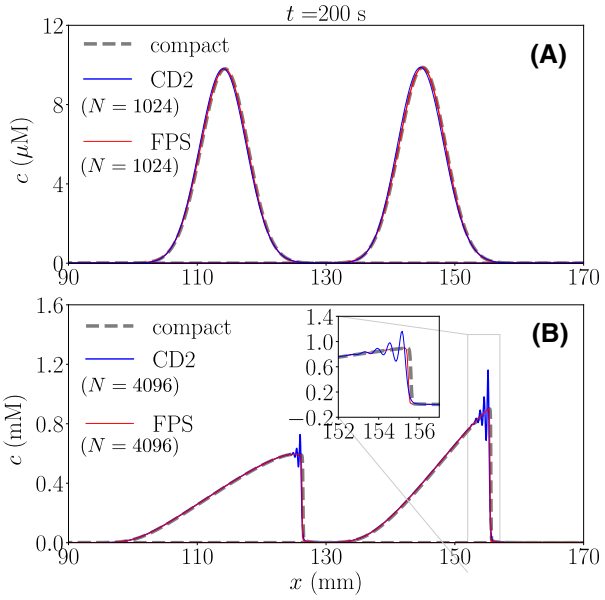

Figure 1. Simulations of electromigration dispersion in CZE using the FPS method and the CD2 scheme, and their verification with SPRESSO simulations based on sixth-order compact scheme with adaptive grid refinement. (A) For low initial concentrations of analytes (10 μM), FPS method and CD2 method yield qualitatively similar peak concentrations. (B) At higher initial concentrations of analytes (1 mM), electromigration dispersion is observed, which is accompanied by sharp concentration gradients. The CD2 scheme fails to resolve the sharp gradients and results in spurious oscillations, as shown in the inset. The FPS method yields a stable nonoscillatory solution for the same number of grid points ($N = 4096$). For both the cases, the concentration profiles simulated using the FPS method agree with those predicted by the compact scheme implemented in SPRESSO.

FPS method and the CD2 scheme yield qualitatively similar nonoscillatory solutions. However, for higher analyte concentrations, shown in Fig. 1B, where electromigration dispersion is observed the CD2 scheme results in spurious oscillations. In contrast, for the same number of grid points, the FPS method is able to resolve the sharp concentration gradients and yields a nonoscillatory solution. For both the cases, the concentration profiles simulated using the FPS method agree with those predicted by the compact scheme implemented in SPRESSO, thereby verifying the implementation of the pseudo-spectral method in our SPYCE simulator.

To compare the accuracy of the FPS method and the CD2 scheme, in Fig. 2 we compare the simulated velocity of pyridine peak for the linear case (with 10 μM initial analyte concentrations) with the theoretical peak migration speed, for varying number of grid points N. The theoretical peak migration speed is given by μE, where E is the electric field in the channel which remains unperturbed due to the migration of low-concentration analytes. As shown in Fig. 2, the FPS method predicts the peak velocity with an error less than 1% with only $N = 128$ grid points, whereas the CD2 scheme requires at least $N = 512$ grid points to achieve comparable accuracy. In Fig. 2, we also present the computational time for simulating the case with 10 μM initial analyte concentrations

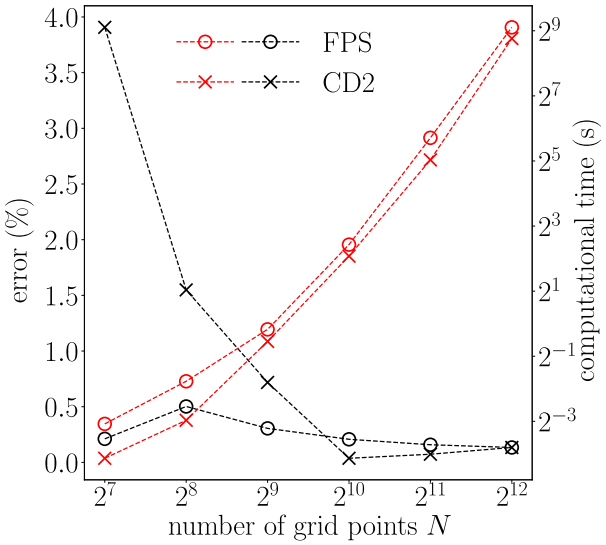

Figure 2. Comparison of the accuracy and computational time of FPS method and CD2 scheme for simulating the linear CZE case with 10 μM initial concentrations of analytes. Shown here is the comparison of the simulated velocity of the pyridine peak with the theoretical value. The FPS method yields higher accuracy than the CD2 method for a smaller number of grid points. The FPS method requires about two times longer computational time than the CD2 scheme for the same number of grid points. However, for the same level of accuracy, the FPS method takes lesser computational time that the CD2 scheme.

for varying number of grid points N. The computational time taken by the FPS method and the CD2 scheme show similar scaling with N. Figure 2 shows that, despite the computational efficiency of FFT algorithm, the FPS method takes about two times longer to simulate the linear CZE problem than the CD2 scheme, for the same number of grid points. However, the higher computational cost of the FPS method is offset by its higher accuracy. For example, the central difference scheme requires at least N =512 grid points and computational time of 1 s (or higher) to achieve an error less than 1% in the peak velocity. In contrast, the pseudo-spectral method yields same accuracy for N =128 grid points (or higher) for which it requires only 0.1 s of computational time, which is over 10-fold speed-up over the central difference scheme. Therefore, the FPS method yields higher accuracy for a coarser computational grid and correspondingly smaller computational time. Although the computational time required for the linear CZE problem is small, simulations of nonlinear electrophoretic processes with sharp gradients require a large number of grid points and relatively longer computational times. The requirement of a coarse grid by the FPS method and corresponding reduction in computational time is particularly beneficial for such nonlinear simulations.

3.2 Transient isotachophoresis (t-ITP)

Next, we consider an example of preconcentration and separation of two analytes using t-ITP. In the configuration of t-ITP that we consider, the analytes are initially injected between the leading electrolyte (LE) and trailing electrolyte (TE) zones. In addition, LE is injected behind the TE zone to affect analyte separation [14]. Upon application of the electric field, the analytes focus and preconcentrate between the LE and TE zones. At a later time, the LE ions behind the TE zone overtake the TE ions and disrupt ITP focusing, thereby initiating electrophoretic separation. This problem was chosen to test whether the FPS method can resolve the sharp concentration gradients in t-ITP. To this end, we performed simulations using the FPS method and the CD2 scheme in a 25 mm long computational domain discretized with 2048 grid points. The LE ion was 50 mM sodium ($pK_a = 13.7$ and $\mu = 51.9 \times 10^{-9}$ m^2/Vs), TE ion was β-alanine ($pK_a = 3.3$ and $\mu = 36.0 \times 10^{-9}$ m^2/Vs), and the background counterion was 100 mM acetic acid. The same composition of LE was used for creating a zone of LE behind the TE zone to affect t-ITP separation. The analytes, pyridine (S1) and aniline (S2), were injected between the LE and the TE zones in the form of Gaussian peaks with peak concentrations of 10 mM. These simulations were performed for a constant current density of 1528 A/m^2, corresponding to a current of approximately 3 μA through a 50 μm diameter circular capillary. Although the accuracy of FPS method is higher than the compact scheme, to verify our numerical implementation, we also performed simulations using the sixth-order compact scheme with adaptive grid implemented in SPRESSO (with 1000 grid points).

The initial concentration distribution of all the species is shown in Fig. 3A. Figure 3B and C shows the concentration profiles of various species during the preconcentration step ($t = 2$ s) and separation step ($t = 150$ s), respectively. The ITP preconcentration step is characterized by sharp concentration gradients, while the gradients during the separation step are relatively small. The FPS method accurately resolves these concentration gradients and the simulated concentration profiles agree with those predicted by the compact scheme of SPRESSO. On the other hand, the CD2 scheme exhibits nonphysical oscillations during the preconcentration step, as shown in Fig. 3B. However, these spurious oscillations vanish during the separation step, which is characterized by relatively low concentration gradients, as shown in Fig. 3C.

3.3 Oscillating electrolytes

Lastly, we present a simulation of an oscillating electrolyte system [10,11] consisting of sebacic acid and imidazole. As shown by Hruška et al. [10], for a particular range of concentrations of sebacic acid and imidazole, small disturbances in initially uniform concentration field amplify under the effect of electric field and result in propagating, oscillatory modes in concentrations. This problem is naturally periodic and can be solved using a periodic computational domain that is much smaller than the actual channel. For these simulations, we took a 25 mm long computational domain discretized with 2048 grid points. The initial state has 0.21 mM sebacic acid ($pK_{a,-2} = 5.38$, $pK_{a,-1} = 4.53$, $\mu_{-2} = -44.9 \times 10^{-9}$ m^2/Vs,

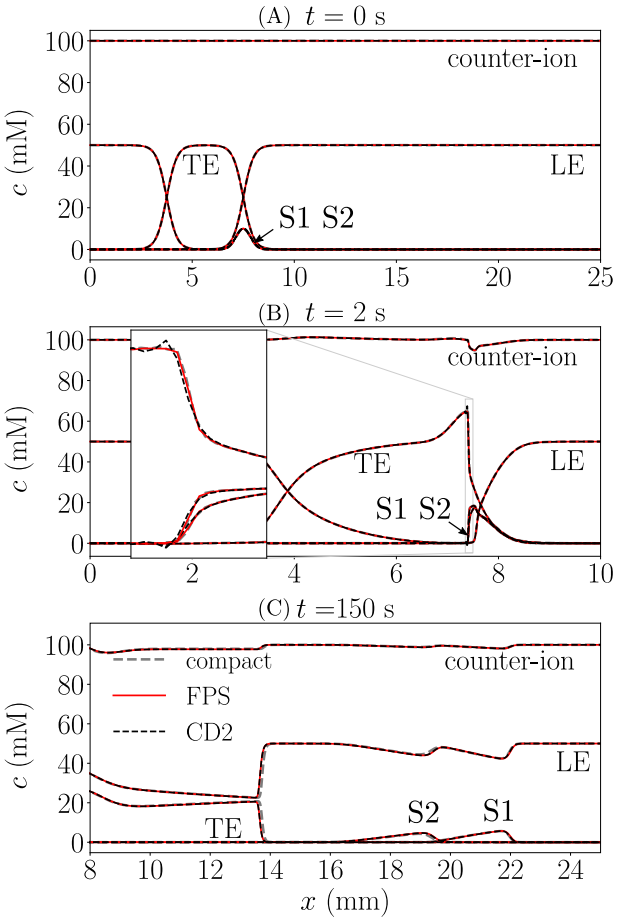

Figure 3. Simulations of t-ITP using the FPS method and CD2 scheme showing coupled ITP preconcentration and electrophoretic separation of two analytes. For verification, also shown are the concentration profiles simulated using SPRESSO employing the sixth-order compact scheme with adaptive grid refinement. The FPS method yields stable solution for both preconcentration (B) and separation (C) steps, and the simulation concentration profiles agree with those predicted by SPRESSO. However, owing to sharp concentration gradients during the ITP preconcentration step (B), the CD2 scheme results in spurious oscillations for the same number of grid points as that for FPS method ($N = 2048$). The simulations using both SPYCE and SPRESSO took about 5 min to run.

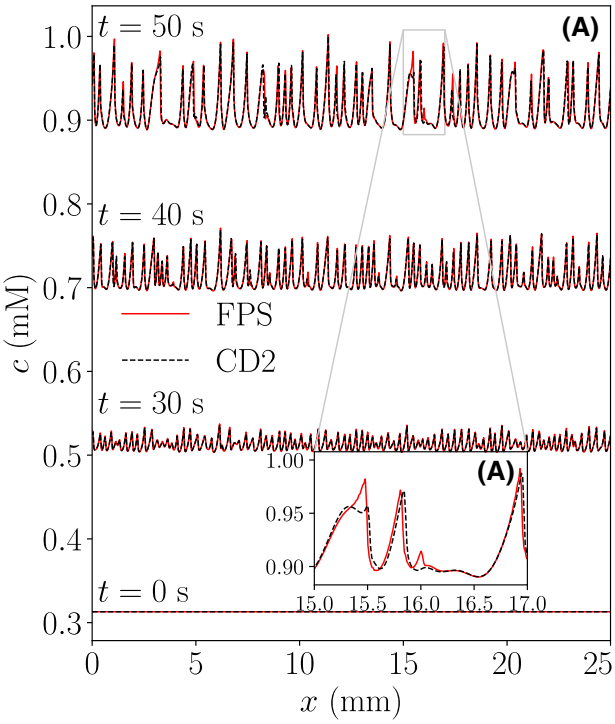

Figure 4. Spatiotemporal evolution of oscillations in imidazole concentration in an oscillatory electrolyte system having a base-state of 0.21 mM sebacic acid and 0.313 mM imidazole, as predicted by FPS and CD2 methods. The concentration profiles are shown at $t = 0$, 30, 40, and 50 s with a vertical offset of 0.2 mM between each plot for illustration. (B) The concentration waves predicted by the CD2 scheme appear to be diffused in comparison with those predicted by the FPS method.

and $\mu_{-1} = -20.7 \times 10^{-9}$ m^2/Vs) and 0.313 mM imidazole (p$K_a = 7.15$ and $\mu = 52.0 \times 10^{-9}$ m^2/Vs) distributed uniformly along the channel axis. To this uniform base-state, we added small random perturbations to the imidazole concentration, modelled by Gaussian white noise with zero mean and standard deviation of 10^{-5} times the base-state concentration of imidazole. The same random perturbation was used for simulations with FPS and CD2 methods to draw a comparison. A constant current density of 100 A/m^2 was applied through the channel with electric field pointing towards the left.

Figure 4 shows the spatiotemporal evolution of oscillations in imidazole concentration, simulated using the FPS method and the CD2 scheme. The initial random perturbations in the concentration field of imidazole amplify exponentially and give rise to deterministic oscillations in the concentrations of both species; here, we present concentration profiles of imidazole only. Over time, the growth of oscillatory modes saturates, and thereafter the individual waves interact with each other without further increase in amplitude. In this case, both the numerical schemes yield stable solution, and these are in qualitative agreement with a similar simulation presented by Hruška et al. [10]. As shown in Fig. 4B, compared with the results from the FPS method, the simulations using the CD2 scheme show relatively diffused concentration waves. This is because the pseudo-spectral method is able to resolve a larger range of wavenumbers than other finite difference schemes for the same computational grid. As shown previously by Gupta and Bahga [11], the growth rates of oscillatory modes are affected by the relative positions of peaks of imidazole and sebacic acid, which themselves depend on the wave propagation velocities. Hence, the FPS method that captures wave propagation more efficiently (higher accuracy for coarser grids) is better suited for this problem.

Furthermore, we note that in this simulation, the concentration gradients are distributed throughout the computational domain. For such problems, the use of

adaptive-grid refinement does not offer significant benefit in improving the simulation accuracy as high grid density is required throughout the domain. The adaptive-grid refinement methods are helpful only for problems where grid points from low-gradient regions can be moved to a few regions with high-concentration gradients. The FPS method is perfectly suited for such problems as it provides high accuracy even on a uniform coarse grid.

4 Concluding remarks

We have demonstrated the application of the Fourier pseudo-spectral method for simulating a wide variety of electrophoretic processes including CZE, t-ITP, oscillating electrolytes, and FASS. We have implemented this numerical scheme in a new electrophoresis simulator, named SPYCE, and verified it with available electrophoresis simulators. Through various examples, we have demonstrated that the Fourier pseudo-spectral method yields high accuracy on coarser computational grids and correspondingly lower computational time to achieve the same level of accuracy. For realistic electrophoresis problems with current densities as high as 5000 A/m^2, the Fourier spectral method offers over10-fold speed-up compared with the commonly used second-order central difference scheme. Moreover, for simulation of nonlinear electrophoretic processes involving sharp concentration gradients, the second-order central difference scheme results in spurious oscillations, while the pseudo-spectral method is able to resolve steep gradients and yields stable nonoscillatory solutions.

We have shown that the Fourier pseudo-spectral method is an excellent alternative to other dissipative and nondissipative spatial discretization schemes for simulating electrophoresis which suffer from low-accuracy and less stability, respectively. The Fourier pseudo-spectral method presented in this work is applicable only for electrophoresis problems that can be simulated in a periodic framework, wherein the initial electrolyte composition at the both ends of the computational domain must be identical. Although we have shown that a wide range of electrophoresis problems can be solved in a periodic framework, a few electrophoretic techniques, such as ITP, moving boundary electrophoresis, and IEF, cannot be simulated on a periodic grid. Such nonperiodic problems can be solved using polynomial based pseudo-spectral methods such as the Chebyshev pseudo-spectral method. We will report the application of such methods for simulating nonperiodic electrophoresis problems in the near future. Nevertheless, as shown in this article, for a wide range of electrophoretic processes, the Fourier pseudo-spectral method offers significant advantages over other numerical schemes. We also note that the Fourier spectral method can offer even greater benefits in terms of computational speed for high-resolution electrophoresis simulations in two- and three dimensions. With freely available FFT libraries for various programming languages and the open-source code of SPYCE, the Fourier pseudo-spectral method can be easily implemented in existing electrophoresis simulators for performing fast and high-resolution simulations.

Data availability statement

Data available on request from the authors.

S.S.B. gratefully acknowledges the financial support received from the Science and Engineering Research Board (SERB), Government of India, under Impacting Research Innovation and Technology (IMPRINT-2) Scheme (Grant No. IMP/2018/000422).

The authors have declared no conflict of interest.

5 References

[1] Jorgenson, J. W., Lukacs, K. D.,*Science* 1983, *222*, 266–274.

[2] Everaerts, F. M., Beckers, J. L., Verheggen, T. P., *Isotachophoresis: Theory, Instrumentation and Applications*, Elsevier, Amsterdam 2011.

[3] Beckers, J. L., Boček, P., *Electrophoresis* 2000, *21*, 2747–2767.

[4] Bharadwaj, R., Santiago, J. G., *J. Fluid Mech.* 2005, *543*, 57–92.

[5] Righetti, P. G., *Isoelectric Focusing: Theory, Methodology and Application*, Elsevier, Amsterdam 2000.

[6] Bier, M., Palusinski, O. A., Mosher, R. A., Saville, D. A., *Science* 1983, *219*, 1281–1287.

[7] Hruška, V., Jaroš, M., Gaš, B., *Electrophoresis* 2006, *27*, 984–991.

[8] Bercovici, M., Lele, S. K., Santiago, J. G., *J. Chromatogr. A* 2009, *1216*, 1008–1018.

[9] Thormann, W., Breadmore, M. C., Caslavska, J., Mosher, R. A., *Electrophoresis* 2010, *31*, 726–754.

[10] Hruška, V., Jaroš, M., Gaš, B., *Electrophoresis* 2006, *27*, 513–518.

[11] Gupta, P., Bahga, S. S., *Phys. Rev. E: Stat. Nonlinear Soft Matter Phys.* 2015, *92*, 022301.

[12] Bahga, S. S., Chambers, R. D., Santiago, J. G., *Anal. Chem.* 2011, *83*, 6154–6162.

[13] Bahga, S. S., Santiago, J. G., *Electrophoresis* 2012, *33*, 1048–1059.

[14] Bahga, S. S., Santiago, J. G., *Analyst* 2013, *138*, 735–754.

[15] Saville, D. A., Palusinski, O. A., *AIChE J.* 1986, *32*, 207–214.

[16] Mosher, R. A., Dewey, D., Thormann, W., Saville, D. A., Bier, M., *Anal. Chem.* 1989, *61*, 362–366.

[17] Bahga, S. S., Bercovici, M., Santiago, J. G., *Electrophoresis* 2010, *31*, 910–919.

[18] Bahga, S. S., Bercovici, M., Santiago, J. G., *Electrophoresis* 2012, *33*, 3036–3051.

[19] Thormann, W., Zhang, C. X., Caslavska, J., Gebauer, P., Mosher, R. A., *Anal. Chem.* 1998, *70*, 549–562.

[20] Thormann, W., Caslavska, J., Breadmore, M. C., Mosher, R. A., *Electrophoresis* 2009, *30*, S16–S26.

[21] Malý, M., Dovhunová, M., Dvořák, M., Gerlero, G. S., Kler, P. A., Hruška, V., Dubský, P., *Electrophoresis* 2019, *40*, 683–692.

[22] Damián, S. M., Schaumburg, F., Kler, P. A., *Comput. Phys. Commun.* 2019, *237*, 244–252

[23] Dubey, K., Gupta, A., Bahga, S. S., *Electrophoresis* 2019, *40*, 730–739.

[24] Mikkonen, S., Ekström, H., Thormann, W., *J. Chromatogr. A* 2018, *1532*, 216–222.

[25] Martens, J., Reijenga, J. C., Boonkkamp, J., Mattheij, R. M. M., Everaerts, F. M., *J. Chromatogr. A* 1997, *772*, 49–62.

[26] Sounart, T. L., Baygents, J. C., *J. Chromatogr. A* 2000, *890*, 321–336.

[27] Breadmore, M. C., Mosher, R. A., Thormann, W., *Anal. Chem.* 2006, *78*, 538–546.

[28] Trefethen, L. N., Spectral methods in MATLAB, Society for Industrial and Applied Mathematics, Philadelphia 2000.

[29] Boyd, J. P., *Chebyshev and Fourier Pseudo-Spectral Methods*, Dover Publications, Mineola, NY 2001.

[30] Sharan S., Gupta, P., Bahga, S.S., *Phys. Rev. E: Stat. Nonlinear Soft Matter Phys.* 2017, *95*, 023103.

[31] Ehrendorfer, M., Pseudo-spectral numerical weather prediction models, Society for Industrial and Applied Mathematics, Philadelphia 2011.

[32] Carcione, J. M., *Geophysics* 2010, *75*, A53–A56.

[33] Hussaini, M. Y., Zang, T. A., *Annu. Rev. Fluid Mech.* 1987, *19*, 339–367.

[34] Gupta, P., Scalo C., *Phys. Rev. E: Stat. Nonlinear Soft Matter Phys.* 2018, *98*, 033117.

[35] Babskii, V. G., Zhukov, M. Y., Yudovich, V. I., *Mathematical Theory of Electrophoresis*, Springer Science & Business Media, New York 2012.

[36] Ghosal, S., Chen, Z., *Bull. Math. Biol.* 2010, *72*, 2047–2066.

[37] Bahga, S. S., Moza, R., Khichar, M., *Proc. R. Soc. A* 2016, *472*, 20150661.

[38] Hou, T. Y., Li, R., *J. Comp. Phys.* 2007, *226*, 379–397.

[39] Ermakov, S. V., Bello, M. S., Righetti, P. G., *J. Chromatogr. A* 1994, *661*, 265–278.

